Electron bubbles, small-polaron holes, and charge-induced effects in solid deuterium

R. L. Brooks, S. K. Bose, J. L. Hunt, Jack R. MacDonald, and J. D. Poll
Guelph-Waterloo Program for Graduate Work in Physics, University of Guelph Campus, Guelph, Ontario, Canada N1G 2W1

J. C. Waddington
Department of Physics, McMaster University, Hamilton, Ontario, Canada L8S 4M1
(Received 25 March 1985)

The charge-induced absorption spectrum in the fundamental band of solid D_2 under proton-beam irradiation has been measured. Under higher spectral resolution than for previous work, we examine the spectra for both normal and ortho-enriched samples. Timing experiments are presented in which the growth and decay of these spectral features are monitored following onset and termination of beam irradiation, and both spectra and timing as a function of temperature are examined. These experimental results are then interpreted within a model in which electron bubbles and small-polaron holes figure prominently. That at least two different kinds of both positive and negative charge carriers are needed to explain the results seems certain. The identification of the positive molecular-ion species is uncertain but evidence for the probable formation of D_9^+ is presented. The consequences for charge transport are critically examined.

I. INTRODUCTION

The solid hydrogens are the simplest and perhaps most interesting molecular solids known. Many of their fundamental properties have been reviewed by Silvera[1] and very recently by Souers.[2] A theoretical treatment pertaining mainly to the interpretation of optical and microwave absorption experiments is contained in the monograph by Van Kranendonk.[3] The definitive experimental work on the fundamental infrared absorption spectrum of solid deuterium was performed by Crane and Gush.[4]

Interest in the use of solid hydrogen for inertial confinement and magnetic fusion stimulated a sequence of experiments performed with liquid and solid HT, DT, and T_2.[5] The infrared spectrum in the fundamental band of each of these molecules was observed to have at least two additional, unexpected spectral lines when the samples were cooled below 12 K.[6] In addition, these extra spectral lines also occurred in the spectra of HD and D_2 when tritium was present in the sample. Warming the sample above about 12 K was sufficient for these new features to disappear. An interpretation of these features has been presented based on the premise that the tritium radioactivity was causing ionization of the sample, resulting in residual ions in sufficient concentration to Stark shift certain absorption transitions in the nearest neighbors of the host lattice.[7]

One central premise of the proposed explanation was confirmed by irradiating samples of solid D_2 with a 15-MeV proton beam. In that experiment both large absorption features (*A* and *B*) observed in the tritium experiments were seen and an additional strong line (*D*) was observed for the first time.[8] It became clear that the phenomenon could be called "charge-induced absorption" and, except for some intensity differences, was independent of the nature of the ionizing radiation. The subject up to this stage has been reviewed by Hunt and Poll.[9] Further experiments have identified a very broad absorption in the near ir (~ 5600 cm^{-1}) for both deuterium[10] and hydrogen.[11]

In this paper we will present the results of a series of experiments performed on deuterium samples using proton-beam irradiation. The spectra of the fundamental vibration-rotation band under moderately high resolution will be examined for both normal samples and ortho-enriched samples. "Timing" results will be presented in which the growth and decay of the charge-induced features are monitored after onset and termination of particle-beam irradiation. Subsequently the temperature dependence for both spectra and timing experiments will be discussed. Finally, the interpretation of these experiments within the framework of a model which seeks to identify the nature of the localized charges will be presented.

Although some of the experimental details have appeared elsewhere, the following section will summarize those that are relevant to this work.

II. EXPERIMENT

Experiments were performed at the Tandem Accelerator Laboratory of McMaster University. A beam of 15-MeV protons at a current of 1—10 nA from the FN tandem was used for all runs. Micrometer adjustable aperture stops and a mechanically oscillating grid were positioned in the beam line just upbeam from the sample cell. The aperture stops were set to 0.8 cm square while the grid, by intercepting 50% of the incident beam in a uniform fashion, monitored the beam current. Following the grid, the beam passed through 25-μm-thick Ni window which isolated the interior of the sample cell from the beam-line vacuum. After passing through 0.9 cm of solid D_2 in which it lost approximately 8 MeV, the beam was stopped in the electrolytic copper walls of the sample cell.

The cell was cooled by a liquid-He transfer line cryostat (Janis S/T) and the temperature was monitored by a Lake Shore Cryotronics DRC-8 temperature controller upgraded to 0.1-K resolution and accuracy. Temperature adjustment was achieved through a 50-Ω Nichrome wire heater wound around the cold finger, close to the temperature sensor. Since complete experimental control had to be maintained externally to the target room which contained our apparatus, the DRC-8 was modified to allow the use of a ten-turn potentiometer for manual temperature control. A closed-circuit television monitor was used for the external temperature display.

After a short equilibration time, the temperature of the sample with the beam off was accurately measured by the temperature sensor. When the beam was on, however, the sample was warmer than the sensor indicated; with good thermal contact between the frozen D_2 and the cell walls, the maximum temperature gradient that could possibly be maintained is 0.3 K. Poor thermal contact might substantially increase this number but based upon the consistency of data taken with and without the beam, the difference in temperature between the sensor and sample is estimated to be a maximum of 1 K and was most probably of the order of ≤ 0.5 K.

Figure 1 shows the optical arrangement of the apparatus. The lamp was a "Globar" infrared source operating at 200 W which approximates a blackbody of 1100 K. The monochromator was a 0.25-m, $f/4$ interchangeable grating-prism instrument from Perkin Elmer, configured with a 300 lines/mm grating blazed at 2.0 μm. The radiation, chopped at 1 kHz by a tuning-fork chopper at the monochromator exit slit, passed through the sample cell at right angles to the proton-beam line through two sets of sapphire windows. The inner set was mounted to the sample cell with indium O rings and the outer set was cemented into the room-temperature walls of the cryostat shroud. The optical path length of the cell is 1.14 cm, which differs from the path length of the proton beam since the interior volume of the cell is most closely approximated by two intersecting right cylinders of unequal radii and lengths. A filter was used immediately in front of the infrared detector as an order sorter, blocking all wavelengths below 2.5 μm. The signal from a thermoelectrically cooled PbSe detector was amplified by a preamplifier and a lock-in amplifier, the output of which went to a voltage-to-frequency converter and finally to a TN1710 multichannel analyzer operated in multiscaler mode. The tuning-fork chopper provided the reference frequency for the lock-in amplifier.

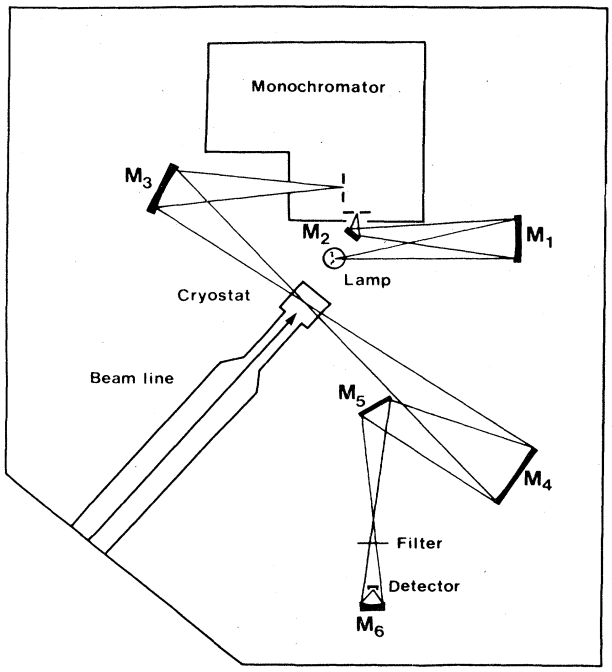

FIG. 1. The experimental arrangement for infrared absorption measurements.

Two different sample cells of interior volume 0.8 cm^3 were employed for these experiments. The cells were identical except for a small additional chamber on one which held a chrome alumina catalyst for para-ortho conversion. Partial conversion was accomplished *in situ* by keeping the cell filled with liquid D_2 in contact with the catalyst for about 2 h. Conversion continued after freezing the sample but at a greatly reduced rate.

III. RESULTS

A. Spectra

For the fundamental band of deuterium, the basic charge-induced features can be observed in Fig. 2. Three absorption lines, labeled A, B, and D, appear only after beam irradiation and only at temperatures below about 12 K. The time frame for growth and decay of these features as well as their temperature dependence will be presented below. The B line is the strongest feature though it appears in the wing of the Q absorption complex. The A line is comparable in magnitude to the D line but the latter is strongly masked by both the Q phonon absorption and the $S(0)$ absorption complex so no detailed experimental studies have been attempted on that feature.

The frequencies quoted previously[8] for the A, B, and D absorption features are 2867(3), 2969(5), and 3139(4) cm^{-1}, respectively. The A-line feature has been attributed to the Stark shifting of the $Q_1(0,1)$ complex by a positive charge. The A line, which has the largest shift, has also been observed in all hydrogenic species except H_2 using radiation from tritium β decay. It was reported[7] that a single ion-molecule separation R of 2.4 Å could explain all of the observed spectral shifts which are different for each of the hydrogens. A more recent calculation[12] indicates that a better value for R in the case of D_2 is 2.3 Å which yields an A-line frequency of 2870.7 cm^{-1}. This value is actually an average of three closely spaced numbers, one from the Stark shift of the $Q_1(0)$ line and two from the $Q_1(1)$. A correction of -7 cm^{-1} required to shift the $Q_1(0)$ transition to its observed position in the solid has been applied to each.

The B and D lines have been attributed, respectively, to Stark-shifted $Q_1(0,1)$ and $S_1(0)$ absorption lines due to a negative charge, i.e., an electron trapped in a bubble.

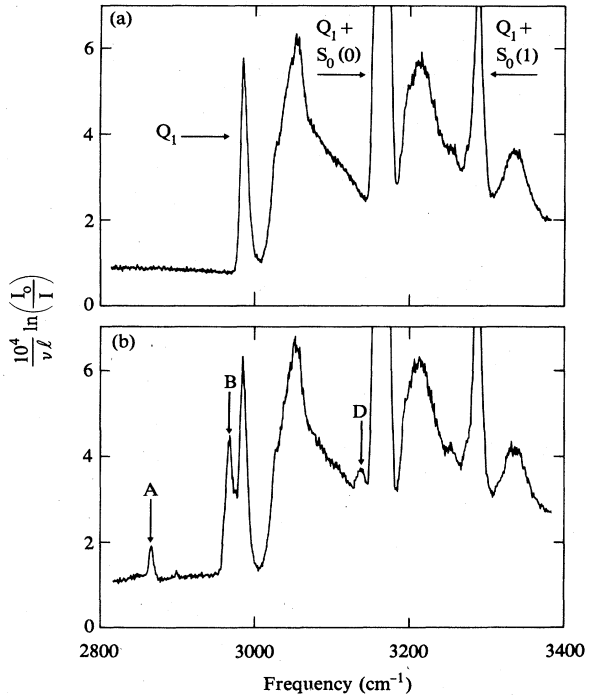

FIG. 2. Absorption features in the fundamental band of solid D_2 at 4.2 K. (a) Beam off. (b) Beam on after 2 min of irradiation at 15 nA/cm^2.

Since this hypothesis was first put forward,[6] further experimental[10] and theoretical[13] work has confirmed the soundness of this proposal so it seems appropriate at this point to reexamine the Stark shifts in somewhat greater detail.

The first question to be addressed is whether a single bubble diameter can predict the measured shifts of the B and D lines. Before the results of the calculation can be applied, the density effects of the solid need to be considered. The $Q_1(0)$ absorption line appears shifted 7 cm^{-1} to a lower frequency than the calculated vacuum value (which agrees with the low-density-gas Raman value) while the $S_1(0)$ line appears 15 cm^{-1} lower than the vacuum value. That these frequency shifts are density-related phenomenon has been confirmed from studies of the gas at high pressure. If one simply takes the calculated vacuum values for the Stark shifts and adds them to the corrected solid values for the $Q_1(0)$ and $S_1(0)$ lines, crude agreement with experiment is obtained; i.e., a bubble radius in the range of 4.5–5.3 Å gives agreement for both lines. Interestingly, the rate of change of the calculated Stark shifts near $R=5$ Å as a function of R for the negative charge is opposite for the B and D lines.[12] If one assumes that the presence of a bubble which is significantly larger than the unperturbed intermolecular distance creates a local increase in the pressure, then an additional negative vibrational shift might be expected. Using an additional shift of -9 cm^{-1}, self-consistency for both the B and D lines is obtained for a charge-molecule separation of 5.1 Å. We interpret this value as an estimate of the bubble radius though clearly such an estimate is an upper bound since the radius of an unperturbed molecule (~ 1.8 Å) should be subtracted from this value.

Such considerations will also apply to the case of the positive charge. Since the lattice is strongly polarized and contracted, a density-dependent correction in the same direction as for the negative charge should apply. However, since the charge-molecule separations are small, the Stark shifting is large and a change of separation from 2.3 to 2.4 Å can accommodate a shift of -20 cm^{-1}.[12] Such a correction could not then significantly alter the estimate for the charge-molecule separation for positive charges, nor would it remove the general agreement obtained for the A-line Stark shifts over all of the hydrogen molecular species.

When the B line is examined under higher spectral resolution, structure becomes apparent. Such is not the case for the A line which can be fitted quite adequately by a single Gaussian component. For this reason we have chosen to deconvolute the B-line—Q-line complex into Gaussian components as well. This will readily permit a comparison to be made between two spectra without there being any implication that the chosen line shape is optimum.

Figure 3 and 4 show the B-Q complexes with a spectral resolution of 1 cm^{-1}. Figure 3 is for a sample of normal deuterium (67% ortho) while Fig. 4 is for a sample of ortho-enriched deuterium ($\sim 85\%$ ortho). Note the dramatic change in the appearance of the Q line which has been extensively studied in the past and is reasonably well understood.[4] The integrated intensity of the Q complex decreases with increasing ortho ($J=0$) concentration because the $Q_1(0)$ transition requires the presence of a $J=1$ neighbor in order to have a nonzero transition moment. Such is not the case for the charge-induced transitions which show almost no change in integrated intensity.

In Fig. 4 the Q_1 transition has been resolved into its components of known frequency allowing the frequencies of the B-line components to be accurately determined. Table I lists the frequencies and integrated intensities of the B-line components for both the normal and ortho-enriched samples. Two components dominate the B line and represent over 85% of the total intensity. Surprising-

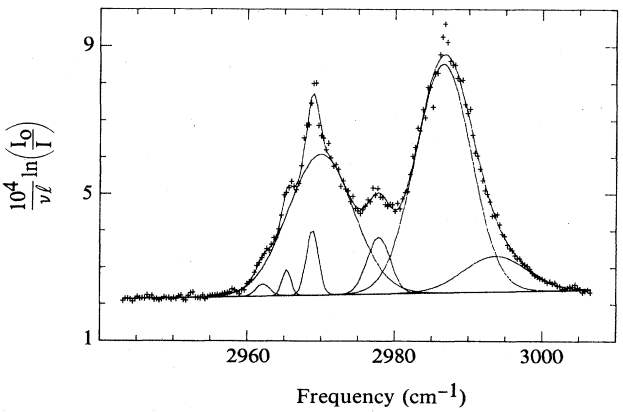

FIG. 3. A high-resolution absorption spectrum of the B-line—Q-line complex for normal D_2 at 4.2 K.

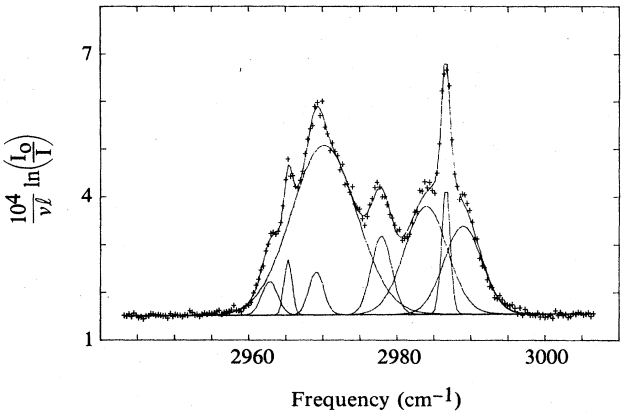

FIG. 4. A high-resolution absorption spectrum of the B-line—Q-line complex for ortho-enriched ($\sim$85%) D_2 at 4.2 K.

ly, very little variation in integrated intensity can be observed between the two samples.

The Stark-shift calculation, when applied to this transition, predicts at most five components; one from the $Q_1(0)$ $\Delta M=0$, two from the $Q_1(1)$ $\Delta M=0$, and two from the $Q_1(1)$ $\Delta M=\pm 1$ transitions. These latter two fall far from the region of the B line where no absorption lines have been observed. Of the remaining three transitions only one originates from ortho deuterium, the $Q_1(0)$ $\Delta M=0$, and hence should be associated with the strongest observed transition at 2970.4 cm^{-1}. The predicted separations among these three transitions are rather insensitive to the choice of the charge-molecule separation and occur at ± 4 cm^{-1} from the shifted position of $Q_1(0)$. The calculation, then, predicts a triplet of lines in which the two outer components decrease in intensity relative to the central component as the ortho concentration is increased; this is not the behavior that is observed.

There is another consideration that argues against the B-line structure being caused by different Stark-shifted levels. The molecules in the vicinity of an electron bubble would be subject to a strong magnetic field gradient from an unpaired electron. In such a field, local conversion to the ortho state should occur rapidly, thereby reducing the available transitions to just the $Q_1(0)$. If that were the case, one would not expect to see any $\Delta M=\pm 1$ transitions and furthermore there would be no structure to the A line since a positive ion would also induce local conversion. No structure in the A line has been observed but our spectral resolution is about the same magnitude as the predicted spread in the Stark-effect structure for this line so it is difficult to be definitive about this point.

The structure in the B line must then be attributed to nonuniformity among the electron bubbles. Since the mechanism for trapping and thereby localizing the electrons depends on lattice vacancies or impurities,[13] it seems reasonable to assume that the bubbles might not be spherical and their sizes and shapes could differ by small amounts. The spectrum, obtained in the vicinity of 5000 cm^{-1}, which has been attributed to excitation of the electron bubbles also shows structure.[10] We have previously attributed this structure to geometrical differences among electron bubbles.

TABLE I. Frequencies and integrated intensities of the B-line—Q-line spectral components. (Line frequencies within ± 0.2 cm^{-1}.)

Normal D_2		$\sim$85% ortho D_2	
ν (cm^{-1})	$\tilde{\alpha}^a$ (cm^{-1})	ν (cm^{-1})	$\tilde{\alpha}^a$ (cm^{-1})
2962.4	$0.8\pm0.3\times10^{-4}$	2963.1	$1.9\pm0.3\times10^{-4}$
2965.6	1.0±0.4	2965.6	1.6±0.3
2969.1	3.7±0.7	2969.4	2.3±0.8
2970.2	42.3±2.2	2970.4	39.0±2.2
2978.1	6.0±0.7	2978.2	5.6±0.6
2986.8	58.8±1.5	2984.2[b]	16.3±1.3
2993.9	10.4±0.8	2986.9[b]	3.9±0.4
		2989.2[b]	11.8±0.8

[a]With $k(\nu)\equiv l^{-1}\ln[I_0(\nu)/I(\nu)]$, $\tilde{\alpha}\equiv\int[k(\nu)/\nu]d\nu$.
[b]Values taken from Ref. 4 and used for calibration.

B. Timing

The principal advantage to using an ion beam over tritium irradiation for studies of the solid hydrogens is that the beam can be turned on and off. We have performed a large number of timing experiments on the A, B, and D lines of solid D_2 in which the intensity is monitored as a function of time after onset and termination of the beam. Such experiments can help to clarify the nature of the charge carriers, their equilibrium concentrations, and their mobilities. Model-dependent calculations of such parameters are discussed in Sec. IV.

The timing experiments were of two types. For the first type the spectrometer was adjusted to the position of maximum absorption and the intensity of the transmitted light was sampled in half-second increments. The run was started with the beam off using an annealed sample. After 10 sec the beam was turned on and the intensity monitored for a predetermined time, typically 15—30 min. The beam was then turned off while still monitoring the intensity for a second predetermined time, usually 30 min. Such type-I measurements yield what we call the "short-time" behavior of the phenomenon.

For the second type of measurements (type II), spectra were acquired as a function of elapsed beam time starting with an annealed sample. The beam was turned off briefly to reset the spectrometer between runs; however, the beam-off time was small relative to the total irradiation time. In addition to beam-on timing runs spectra were also acquired as a function of time after terminating the beam. The time required to scan over a line (10—15 sec) was short compared to the time scale of the experiment (hours) and has been ignored. The great advantage to taking spectra as a function of time is that the integrated intensity of the absorption feature can be obtained which removes any background effects. One such background effect appears to be an overall extinction, probably from scattering, which seems to be uniform over the entire spectral range studied. The extinction increased whenever the beam was on the sample. Over several hours of beam exposure at 8 nA/cm^2, the clarity of a sample degraded

until the transmission was unacceptably poor. The sample was then melted and a new polycrystal was formed.

Figure 5 and 6 show the results of timing experiments for the *A*, *B*, and *D* lines at 4.2 K with a beam current of ~ 8 nA/cm^2. The scattered points are integrated intensities from timing spectra of type II described above. The solid curves obtained over the first 30 min are composite rescaled multiexponential fits to timing experiments of type I. The fitting parameters have been chosen so that for times greater than 30 min the curves agree with the scattered points. The solid curves, thus, represent our best experimental determination of the timing behavior of these charge-induced spectral features. The broken curves are model-dependent fits to the data which will be explained in Sec. IV.

When timing experiments for different polycrystals are compared, substantial differences occur in the multiexponential fitting parameters. We do not believe that the experiments are sufficiently refined for any interpretation to be given to the specific lifetimes extracted from these multiexponential fits. However, the overall time scale, as well as a separation into long and short components, can be obtained for each of the spectral features for both turn-on and turn-off of the beam and all of this is well represented by the solid curves in the figures.

Note that the behavior of the *B* and *D* lines are similar for both beam-on and beam-off experiments. By contrast the *A*-line turns on about a factor of 10 more slowly than either of the others and most strikingly shows no decrease in intensity over 4 h after the beam has been turned off at 4.2 K. Clearly there is an apparent reversal in the intensity ratios of the *A* and *B* lines after a long time. An interpretation of these experiments will be given after the temperature dependence has been presented.

C. Temperature dependence

With the beam turned off, all of the charge-induced spectral features can be eliminated by warming the sample above about 12 K. This temperature is still well below the melting point (18.6 K) and we make use of this property to anneal the sample between short-term timing runs (type I).

The spectra of Fig. 7 show the disappearance of the *A* line with increasing temperature. For this experiment the sample was irradiated at 4.2 K for about 15 min, after

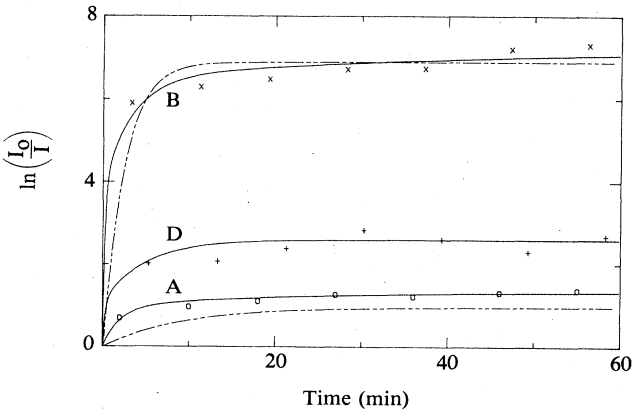

FIG. 5. Turn-on timing curves for *A*, *B*, and *D* charge-induced absorption features. Solid curves are multiexponential fits to data and the dashed curves are model-dependent fits as described in the text.

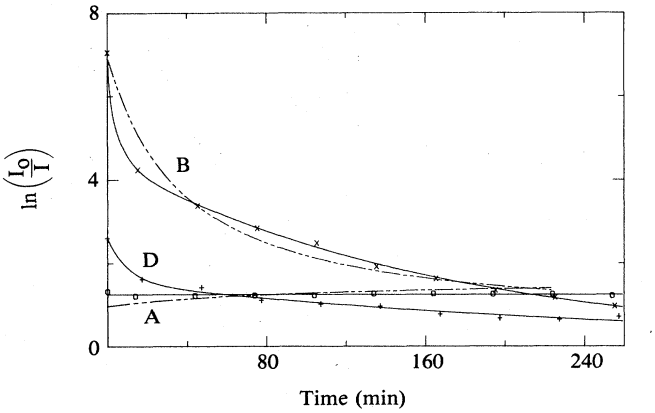

FIG. 6. Turn-off timing curves for *A*, *B*, and *D* charge-induced absorption features. Solid and dashed curves as in Fig. 5.

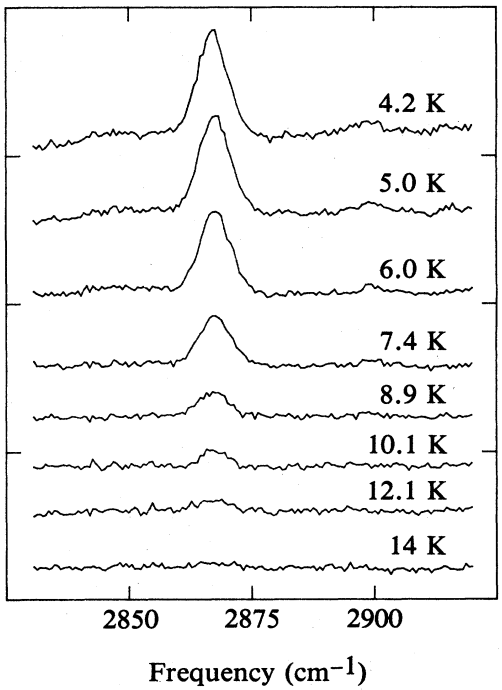

FIG. 7. Temperature dependence of the *A*-line charge-induced absorption feature of solid D_2. Sample irradiated for 15 min at 4.2 K prior to above spectra. The times from beam termination to start of spectra are 4.2 K, 4 min; 5.0 K, 41 min; 6.0 K, 53 min; 7.4 K, 67 min; 8.9 K, 84 min; 10.1 K, 99 min; 12.1 K, 115 min; 14 K, 133 min.

which the beam was turned off and the spectra acquired as a function of temperature. Recall that the A line shows no decrease in intensity with time at 4.2 K. Subsequently we will show that this property persists to at least 6.5 K. Thus we conclude that the observed reduction in A-line intensity is predominantly temperature related.

The corresponding experiment for the B line is shown in Fig. 8. The vertical scale is the same for each curve and the same as that for Fig. 7. Only the arbitrary vertical displacements are different. Two factors which are not present for the A line should be considered. The first is the proximity of the large Q line which has been removed by subtracting a beam-off spectrum from those in the figure. This subtraction produces the noise in the spectra at 2984 cm^{-1}. The second is that the B line is known to reduce in intensity with time after irradiation ceases. We shall show subsequently that this reduction occurs faster as the temperature is raised. Consequently the reversal in ratio of the A- and B-line intensities, which occurs after a long time with the beam off at 4.2 K, can be hastened by simply warming the sample.

Timing experiments (type I) have been performed at a selection of temperatures for both the A and B lines. These experiments suffer from an additional source of error because the temperature of the sample may be somewhat different from the temperature indicated by the sensor when the beam is on the sample. Additionally, when the beam is turned off a rapid manual adjustment to the heater current must be performed to compensate for the cessation of heating by the beam. Despite our best efforts we have sometimes observed the display temperature to drop by 0.3 K when the beam is turned off.

Timing runs for a selection of temperatures are shown in Fig. 9 for the A line and in Fig. 10 for the B line. Zero on the time axis represents the moment that the beam was turned off. When the beam is stopped, both the rapid in-

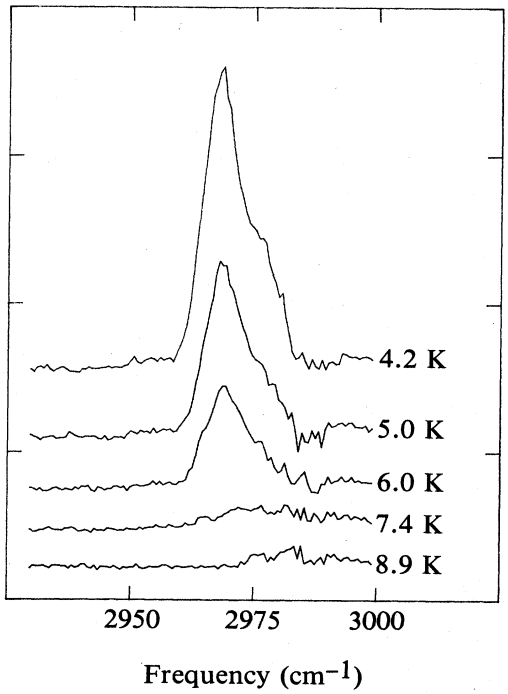

FIG. 8. Temperature dependence of the B-line charge-induced absorption feature of solid D_2. Spectra were acquired as for Fig. 7.

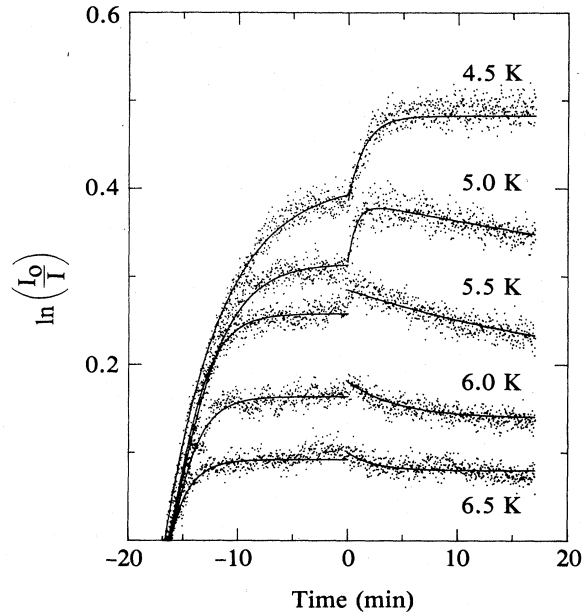

FIG. 9. A-line timing curves at selected temperatures. Proton beam turned off at zero on time axis.

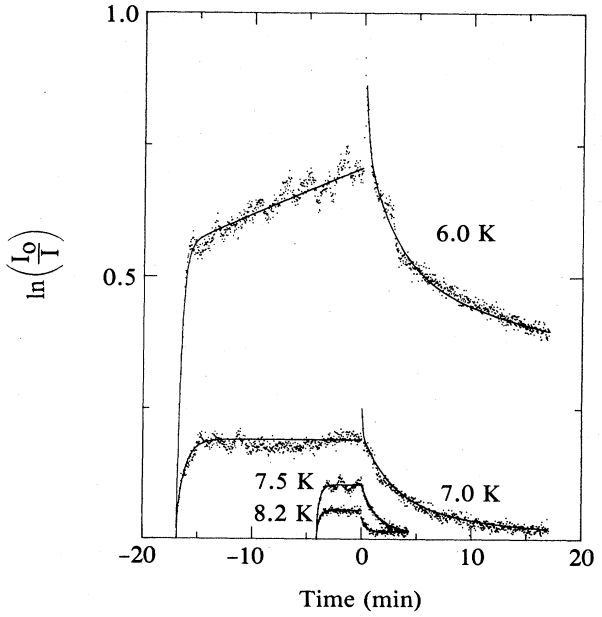

FIG. 10. B-line timing curves at selected temperatures. Proton beam turned off at zero on time axis.

TABLE II. B-line turn-off times. Time needed for intensity to drop to $1/e$ of initial value.

Temperature (K)	Lifetime (sec)
4.2	6000±300[a]
6.0	2100±200[a]
7.0	240±40[a]
7.5	84±5[b]
7.8	36±3[b]
8.2	23±4[b]
9.0	14±6[b]

[a]Multiexponential fits. Value at 4.2 K taken from Fig. 6.
[b]Single-exponential fits.

crease in intensity for the B line and the gradual increase for the A line can be attributed to a temperature change in the sample. From these curves we estimate the maximum temperature error to be 0.5 K.

All of the A-line timing curves were performed at a beam current density of 3 nA/cm^2. The same current density was used for the B-line timing runs at 7.0, 7.5, and 8.2 K. Lower-temperature B-line curves were performed at 8 nA/cm^2. Although two of the A-line curves (at 5.0 and 5.5 K) appear to decrease in amplitude after the beam is stopped, we suspect that this was caused by an unstable sample temperature, particularly since the curves at lower and higher temperature do not show this effect.

Clearly the saturated amplitude of the A- and B-line absorption decreases with increasing temperature. Note that the A line shows no measurable amplitude when an annealed sample is irradiated above about 7 K, while Fig. 7 clearly shows an A line persisting at 12 K when the beam irradiation occurred previously at 4.2 K. More importantly the time to achieve saturation decreases with increasing temperature for both lines. While the A line shows no decrease in amplitude with time for any temperature up to 6.5 K, the turn-off time of the B line shows a dramatic decrease as the temperature is raised. In fact the turn-off times yield the most information regarding the mobilities of charge carriers because the magnitude of the beam current is not a parameter in such measurements. Table II summarizes these lifetimes for the B line.

The set of timing measurements presented in Figs. 9 and 10 as well as the composite results of Figs. 5 and 6 at 4.2 K provide a great deal of information. We have extended and refined a model, initially proposed to explain only the Stark shifts of the spectral features, which can satisfactorily account for all of the observed timing characteristics. This model will be discussed in the following section.

IV. DISCUSSION

A. The standard model

Initially we shall present our "standard" model regarding the nature and number of ions present in the sample. This model utilizes the simplest set of assumptions which can be made to yield timing curves in reasonable agreement with the measured curves of Figs. 5 and 6. Unfortunately, one consequence of this model related to the positive ions appears unreasonable and this point will be discussed in Sec. IV B and an alternate interpretation presented in Sec. IV C.

When a 15-MeV proton beam traverses a 0.9-cm-thick sample of solid D_2 it loses 8 MeV almost entirely to electrons ($\sim$0.05% of the energy is lost in nuclear processes[14]). Since the electron energy-loss mechanism is predominantly ionization, a single proton will create $\sim 10^5$ D_2^+,e^- pairs. The D_2^+ will react strongly with the host via the reaction

$$D_2^+ + D_2 \rightarrow D_3^+ + D \ . \tag{1}$$

We propose that the majority of electrons are mobile but that some become trapped in lattice defects and form localized, immobile bubbles. A proposed mechanism for formation of these bubbles and a calculation of their stability appears elsewhere.[13] Furthermore, we consider the D_2^+ to be mobile (the mechanism will be discussed subsequently) while the D_3^+ are not. The charged species present in the sample during beam irradiation are (1), D_2^+; (2), D_3^+; (3), e_l^-; and (4), e_m^- where the subscripts l and m refer to "localized" and "mobile," respectively. The numbers will permit a simplified notation for the density of each species; e.g., N_1 is the number concentration of D_2^+ ions in cm^{-3}, etc.

If one assumes that the beam creates λ (cm^{-3} sec^{-1}) ion pairs per unit volume per second, then one may write down a set of first-order, coupled, nonlinear rate equations for the concentrations of each of the species. Three such equations plus a fourth for charge conservation are sufficient and may be written

$$\dot{N}_1 = \lambda - \alpha_{14} N_1 N_4 - \gamma_1 N_1 - \alpha_{31} N_3 N_1 \ , \tag{2}$$

$$\dot{N}_2 = \gamma_1 N_1 - \alpha_{24} N_2 N_4 \ , \tag{3}$$

$$\dot{N}_3 = \gamma_4 N_4 - \alpha_{31} N_3 N_1 \ , \tag{4}$$

$$N_1 + N_2 = N_3 + N_4 \ . \tag{5}$$

These equations incorporate the previously mentioned assumptions regarding mobility. In this context we use the term "mobility" to refer to any movement of the charges regardless of cause.

The γ coefficients are production rate constants and may be written as

$$\gamma_1 \equiv \sigma_{1h} v_1 N \tag{6}$$

and

$$\gamma_4 = \sigma_{4h} v_4 N_v \ , \tag{7}$$

where σ_{1h} is the cross section for production of D_3^+ from D_2^+ and the host molecules (D_2), v_1 is the D_2^+ velocity, and N is the concentration of D_2. σ_{4h} and v_4 are analogously defined for the mobile electron, and N_v is the number of vacancies or "seed" positions for electron bubble formation.

The α coefficients are recombination rate constants and are defined as follows:

$$\alpha_{14} \equiv \sigma_{14} v_4 \ , \tag{8}$$

$$\alpha_{31} \equiv \sigma_{31} v_1 \ , \tag{9}$$

$$\alpha_{24} \equiv \sigma_{24} v_4 \tag{10}$$

with σ_{14} the cross section for recombination of a mobile electron and D_2^+, and σ_{31} and σ_{24} are analogously defined. The turn-on behavior is obtained with the initial conditions $N_1 = N_2 = N_3 = N_4 = 0$ and $\lambda \neq 0$. The turn-off behavior is obtained by setting $\lambda = 0$ and each of the N_i values to the equilibrium concentrations obtained by the turn-on solution.

The magnitudes for λ and N will suffice to set the scale for the entire problem. N is known[2] to be 3×10^{22} cm^{-3} at 4.2 K while a reasonable estimate for λ is 3×10^{15} cm^{-3} sec^{-1} for a beam current density of 1 nA/cm^2. The equations were solved numerically for given values of the five α and γ parameters, and these parameters were adjusted until reasonable agreement for both the turn-on and turn-off curves was obtained.

The intensities of the A and B lines are taken to be proportional to N_2 and N_3, respectively. However, as mentioned previously one would expect the A line to be stronger than the B line for equal concentrations since the A line has a larger line-strength factor. We have solved these equations for two different choices of this factor and are able to obtain reasonable agreement for either choice.

The parameters in Table III yield the dashed curves in Figs. 5 and 6. There are five adjustable parameters in the model and five independent "features" to the experimental curves. These are the turn-on and turn-off times of the A and B lines (four features) and the beam-on equilibrium ratios of A- and B-line intensities. For a given assumption regrading the line-strength factor, we expect the solution to be unique.

Clearly all of the dominant features of our data have been fitted by the model. That the A line turns on more slowly than the B line is a consequence of the D_2^+ to D_3^+ conversion rate and the low mobility of D_2^+. That the turn-off times are entirely different from the turn-on times results from there being, in the model, two different kinds of positive and negative charge carriers and, more importantly, that the species causing the observed lines are not the ones directly created by the beam.

While the beam is on, the D_2^+ and e_m^- concentrations build up and stabilize at values at least an order of magnitude larger than D_3^+ and e_l^-. After the beam is turned off the e_m^- concentration is the first to vanish. The D_2^+ concentration is exhausted more slowly leaving only D_3^+ and e_l^- in equal numbers. Under this circumstance the A line is much stronger than the B, which is no longer visible above the noise.

The change in the timing curves as the temperature is raised can be explained as a temperature dependence of the parameters v_1 and v_4. Even the temperature "glitches" as the beam is turned off are reproduced by discontinuously lowering all of the α and γ parameters when λ is set to zero. The dramatic change in the turn-off time of the B line as the temperature is raised can be related through the model to the mobility of D_2^+ in the sample. Before discussing this aspect we shall examine in greater detail some of the consequences of this model.

TABLE III. Model parameters for curves on Figs. 5 and 6 using a line-strength factor of 2; i.e., $I_A/I_B = 2N_2/N_3$.

$\lambda = 10^{16}$/cm^3 sec	$\gamma_1 = 9 \times 10^{-6}$/sec
N_1[a] $\sim 10^{17}$/cm^3	$\gamma_4 = 5 \times 10^{-4}$/sec
N_2[a] $= 5 \times 10^{14}$/cm^3	$\alpha_{14} = 9 \times 10^{-19}$ cm^3/sec
N_3[a] $= 7 \times 10^{15}$/cm^3	$\alpha_{24} = 2 \times 10^{-20}$ cm^3/sec
N_4[a] $\sim 10^{17}$/cm^3	$\alpha_{31} = 6 \times 10^{-20}$ cm^3/sec

[a]Equilibrium beam-on concentrations.

B. Consequences of the model

The equilibrium beam-on concentrations of N_2 and N_3 given in Table III are in good agreement with an order-of-magnitude estimate for the ion concentration needed to produce the A and B lines.[7] It is not so simple to compare model cross sections with measured values since the relative velocities of ions in the solid at these temperatures are unknown. If, however, we eliminate the velocity from Eqs. (6) and (9), the following comparison of two cross sections can be obtained:

$$\sigma_{31} = \frac{\alpha_{31} N}{\gamma_1} \sigma_{1h} = 3 \times 10^8 \sigma_{1h} \ . \tag{11}$$

σ_{1h} is the cross section for D_3^+ formation from D_2^+ in the lattice while σ_{31} is the recombination cross section for D_2^+ and a trapped electron.

Reaction (1) has been extensively studied[15,16] and the cross section measured down to 2 meV.[17] Since for H_2 the reactants are in the ground vibrational and lowest two rotational states even at room temperature, it seems safe to extrapolate values for H_2 down to our temperatures and apply the results to D_2. Hence, σ_{1h} should not be smaller than 10^{-14} cm^2.

The recombination cross section for D_2^+ and an electron has been measured using the merged-beam technique by McGowan *et al.*[18] Although the energy range studied was 0.01—0.08 eV, the authors felt confident enough to extrapolate to 1 meV. Extrapolating to 0.4 meV one may obtain $\sigma_{31} = 5 \times 10^{-13}$ cm^2. It is not at all obvious that this number can be applied to our system in which the electron is trapped in a bubble. One might argue that if the electron wave function were localized, the cross section should be larger. However, we consider it highly unlikely that the cross section could be 7 orders of magnitude larger as is needed to satisfy Eq. (11).

The difficulty seems to reside in Eq. (6). The combination γ_1/N yields a value of $\sim 3 \times 10^{-28}$ cm^3/sec for a reaction whose rate constant at room temperature is $\sim 10^{-9}$ cm^3/sec.[16] Quite simply, the model demands conversion to D_3^+ take place very slowly when it is known to be a highly favored and rapid reaction. Perhaps some inhibiting mechanism is operable in the solid. If not, all of the essential features of the model can be kept by reinterpreting the nature of the positive ions as discussed in the following section.

Before concluding this section, mention should be made of one further consequence of the model which is not in agreement with experimental observations. The results of timing experiments, taken as a function of beam current

at 4.2 K, have appeared previously (Selen *et al.*, Ref. 10). The shorter timing components (<2 min), for beam-on results, were observed to scale inversely with beam current for currents which spanned about 1 order of magnitude. Furthermore, the saturated intensities, for all observed charge-induced phenomena, are independent of beam current over the same order of magnitude.

Model timing curves have been generated as a function of current (λ) which spanned a factor of 20. The turn-on times for the model features scale approximately as $\lambda^{-1/2}$ rather than λ^{-1} which has been experimentally measured. However, the saturated intensities for the model are insensitive to current, in agreement with our measurements.

C. An alternate interpretation

It is possible to keep Eqs. (2)—(5) but change the identities of N_1 and N_2. If conversion to D_3^+ takes place too rapidly to be experimentally resolved, then N_1 could be the D_3^+ concentration while N_2 could be some stable $D_3^+(D_2)_n$ complex which gives rise to the A line. While this possibility has previously been considered,[7] no calculations were available at that time for comparison with the Stark-shift results. Recently such complexes have been theoretically studied for hydrogen, and the lowest harmonic ro-vibrational frequencies have been calculated for H_5^+, H_7^+, and H_9^+.[19] Ions such as these with much higher values of n have been experimentally observed using supersonic nozzle beams and mass-spectrometric techniques.[20] Such experiments have demonstrated that H_n^+ for odd n have intensities 50 times higher than for even n and that H_9^+ and H_{15}^+ are particularly stable.

If such complexes were responsible for the A line, then one might presume that the symmetric D_9^+ (or less likely, D_{15}^+) would be favored in the solid. The D_9^+ molecular ion is composed of a triangular D_3^+ with three D_2 molecules attached to the vertices. The three D_3^+ nuclei and the three D_2 bond midpoints lie in a common plane with the three D_2 internuclear axes perpendicular to this plane.[19] The symmetry group for this molecular ion is D_{3h}. Of course the calculation was performed for H_9^+ and we shall assume its validity for D_9^+.

The lowest harmonic ro-vibrational frequencies for this molecular ion are clearly composed of frequencies identifiable as belonging to the constituent D_2 and D_3^+ partners as well as new frequencies which are peculiar to the complex. The new frequencies all occur in the far infrared so that the only relevant one for our purpose is the fundamental vibrational frequency of the D_2 ligand. The frequency shift between the Q_1 fundamental of the ligand and the Q_1 fundamental of the isolated molecule, both calculated using the same level of theory (called DZ + P SCF[19]), can be compared to the shift calculated using the Stark effect and to the experimental shift. The experimental value of the A-line shift is 109 cm^{-1}. The Stark-shift calculation[12] yields 106 cm^{-1} and the calculation of Yamaguchi *et al.*[19] gives 103 cm^{-1} after dividing the H_9^+ value by $2^{1/2}$ for the isotope change. While such good agreement may be fortuitous it is interesting that the distance from the center of the H_3^+ to the center of one of the H_2 ligands is 2.35 Å. This distance will not be very different for D_2 and is also in good agreement with the Stark-shift value quoted previously. Thus the formation of D_9^+ in our sample by the beam appears probable.

This alternate interpretation admits to rapid formation of D_3^+ in the solid but demands that rearrangement of the nearest neighbors into a complex of appropriate symmetry must take place before the A line can be observed. Since all intermediate species must occur with concentrations too small to be spectroscopically detected one must conclude that there exists some unique complex in the solid preferred over all others which gives rise to the A line. The formation of such a complex with preferred symmetry then accounts for the small value of σ_{1h} in the model. Present experiments cannot determine the symmetry of this complex.

D. Ion mobilities

One aspect of the experimental results not yet considered is the temperature dependence of the phenomenon. Above about 12 K self-diffusion is sufficiently important to prevent any electrons from becoming trapped in bubbles. In the limit that γ_4, the production rate constant for trapped electrons, becomes zero, N_3 is zero and N_2 remains too small for the A line to be visible. For temperatures below about 12 K, diffusion proceeds primarily through vacancy-assisted quantum-mechanical hopping.[21] Our assumption is that γ_4 increases as the temperature decreases, finally allowing the B line to appear above the noise at about 9 K while the A line appears below about 7 K. That the A line can persist to temperatures higher than 7 K with the beam off, after irradiation at 4.2 K, is a natural consequence of the rate equations since γ_4 does not contribute to the decrease of either N_2 or N_3.

At temperatures low enough for both the A and B lines to be visible, we shall assume that diffusion of the bulk D_2 molecules is small enough to ignore. The timing curves are then governed by the mobilities of the ions and electrons.

When the mobilities of excess charge carriers were measured in rare-gas solids[22] it was found that the negative charges had drift mobilities about 5 orders of magnitude larger than the positive charges. When the temperature dependence of the positive charge mobilities was examined the best explanation was obtained by considering the positive charges to be small-polaron holes. When a similar experiment was performed in solid hydrogen[23] it was found that only the negative charges had mobilities large enough to be measurable and these mobilities became so small as the temperature was lowered that no measurements were possible below about 11 K. For the case of solid hydrogen it was suggested that these negative charge carriers might be interpreted as small polarons.

Our experiments were performed at substantially lower temperatures than the above-mentioned conductivity experiments. In view of the fact that our fastest timing features are still of the order of seconds, it is not unreasonable to suppose that what we have termed "mobile electrons" in order to distinguish them from the electron bubbles, are in fact not very mobile and may indeed be small polarons. According to our model the timing feature most directly related to these mobile electrons is

the fast component of the B-line turn-off curves at the lowest temperatures measured.

There is one mobile ion in our model, namely, D_2^+ in the standard version and D_3^+ in the alternate interpretation. Since solid deuterium is a molecular crystal, the ionization process creates some local distortion of the lattice and the positive charge along with its attendant distortion can be treated as a small-polaron hole. Movement of this small-polaron hole is accomplished by hopping to a neighboring site should the distortion patterns happen to be similar. This may occur through zero-point vibration. The higher the symmetry in the neighborhood of a positive charge the less likely it is that the distortion patterns will match and hence the hopping probability, related to what is called the transfer integral, could become vanishingly small around those sites which give rise to the A line. The concept of a small-polaron hole might then be applied to our experiment irrespective of the interpretation attributed to the positive ions. We shall try the same analysis as that performed by Le Comber *et al.* for the rare-gas solids[22] and for solid hydrogen.[23]

The timing feature most closely related to the mobile positive ion is the slow component of the B-line turn-off at low temperatures which for temperatures above 6.5 K becomes the sole single-exponential component. If one makes the assumption that these turn-off times are inversely proportional to the positive-ion mobility, one may plot relative mobilities (on a logarithmic scale) versus inverse temperature as in Fig. 11. Both solid curves are fits to the nonadiabatic theory of Holstein[24] as applied in Ref. 22. The straighter curve ignores the data point at 4.2 K. The mobility may be written

$$\mu(T)=\frac{A}{T}\sinh^{1/2}(\Theta/2T)\exp[-2\gamma\tanh(\Theta/4T)]\ . \tag{12}$$

The constant coefficient A, which is related to the transfer integral, J, between hopping sites, is indeterminate in this analysis; $\Theta=\hbar\omega_0/k$ where ω_0 is some characteristic phonon frequency and $\gamma=E_b/\hbar\omega_0$ where E_b is the polaron binding energy.

The curve which fits all of the data yields $\hbar\omega_0=3.8$ meV and $E_b=130$ meV. However, the point at 4.2 K may be beyond the limit of applicability of the theory. Without this point one obtains $\hbar\omega_0=1.1$ meV and $E_b=24$ meV in good agreement with the numbers obtained in solid hydrogen for small polarons.[23] (One might expect these numbers to be similar for deuterium. Of course the transfer integral J and hence the mobility itself may be very different for polaron holes in deuterium than for polarons in hydrogen.) Unfortunately this curve predicts a B-line lifetime at 4.2 K of 12 days which is about 2 orders of magnitude larger than the measured one. Given the assumptions underlying Fig. 11 and the approximations inherent in the theory (e.g., one dimensional) it seems imprudent to push this analysis any further. One might conclude that our data are probing the breakdown region for the theory. Nevertheless, good agreement can be obtained between about 6 and 9 K, which may be indicative of the presence of small-polaron holes in solid deuterium.

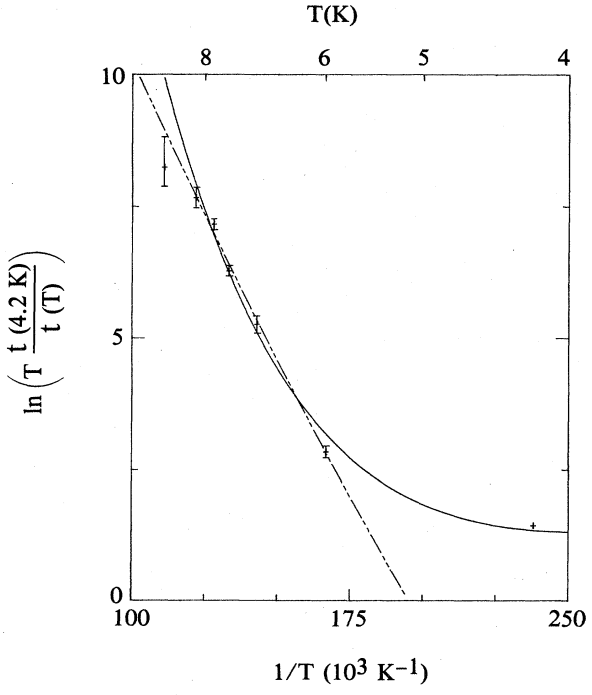

FIG. 11. Logarithm of ion mobilities vs inverse temperature for beam-off lifetime data of B line quoted in Table II.

V. CONCLUSIONS

Proton-beam irradiation of solid deuterium produces extra spectral features in the fundamental absorption band which we refer to as charge-induced effects in the spectrum. These effects can be explained as Stark-shifted features of the normal spectra if one considers the beam irradiation as building up a substantial concentration of ions in the sample. The nature of these ions is uncertain but two important clues can be deduced from our timing experiments. The first is that the ions causing the spectral features have extremely low mobilities and the second is that these ions cannot be directly formed by the beam.

A model has been presented in which two positive and two negative charges are involved to explain the timing results. One of each is extremely immobile and has been interpreted as an electron bubble for the negative charge and either D_3^+ or perhaps more plausibly $D_3^+(D_2)_n$ for the positive charge (with $n=3$ perhaps). The more mobile specifies have been interpreted as electrons (possibly as small polarons) and small-polaron holes (either D_2^+ or D_3^+). While the overall features of our timing experiments can be explained by this model, individual lifetime components differ from experiment by as much as an order of magnitude and hence a four-component model is almost certainly too simple.

Under higher spectral resolution from previous work we have discovered structure in the B line which is not present in the A line and have compared this structure in normal D_2 to that in ortho-enriched D_2. Surprisingly, the structure is nearly identical in both samples thereby ex-

cluding the possibility of its being caused by the resolution of individual Stark components.

The temperature dependence of the charge-induced effects has been examined and found to be consistent with what is known about self-diffusion and ion mobilities in solid deuterium. However, very few prior measurements of these phenomena have been performed in the temperature range of 4.2—9 K, where most of our measurements have been taken.

That charge-induced effects are common to all of the hydrogen isotopes has already been established. If the interpretation of these effects as caused by large concentrations of immobile ions is correct then further experiments are required to try to identify the nature of the charged species. The question of whether such effects can be observed in other molecular solids is one that we also hope to address.

ACKNOWLEDGMENTS

We would like to thank Mats Selen, Kartik Shanker, and Dianne Arlen for their help with data collection, and D. Emin for helpful conversations. We also thank the technical support staff at the McMaster University Tandem Accelerator Laboratory as well as Gord Willis and Tom Riddolls at the University of Guelph. We gratefully acknowledge financial assistance from the Natural Sciences and Engineering Research Council (NSERC) of Canada in the form of an infrastructure grant to support the accelerator laboratory and for individual operating grants.

[1]I. F. Silvera, Rev. Mod. Phys. **52**, 393 (1980).

[2]P. C. Souers, *Properties of Hydrogen for Fusion Engineers* (University of California, Berkeley, in press); Lawrence Livermore Laboratory Report No. UCRL-52628 (1979) (unpublished).

[3]J. Van Kranendonk, *Solid Hydrogen* (Plenum, New York, 1983).

[4]A. Crane and H. P. Gush, Can. J. Phys. **44**, 373 (1966).

[5]P. C. Souers, D. Fearon, R. Garza, E. M. Kelly, P. E. Roberts, R. H. Sanborn, R. T. Tsugawa, J. L. Hunt, and J. D. Poll, J. Chem. Phys. **70**, 1581 (1979); P. C. Souers, J. Fuentes, E. M. Fearon, P. E. Roberts, R. T. Tsugawa, J. L. Hunt, and J. D. Poll, *ibid.* **72**, 1679 (1980).

[6]P. C. Souers, E. M. Fearon, P. E. Roberts, R. T. Tsugawa, J. D. Poll, and J. L. Hunt, Phys. Lett. **77A**, 277 (1980).

[7]P. C. Souers, E. M. Fearon, R. L. Stark, R. T. Tsugawa, J. D. Poll, and J. L. Hunt, Can. J. Phys. **59**, 1408 (1981).

[8]R. L. Brooks, M. A. Selen, J. L. Hunt, Jack R. MacDonald, J. D. Poll, and J. C. Waddington, Phys. Rev. Lett. **51**, 1077 (1983).

[9]J. L. Hunt and J. D. Poll, in *Proceedings of the NATO Conference on Induced Effects, Bonas, France, 1983* (Plenum, New York, in press).

[10]J. H. Richardson, S. B. Deutscher, P. C. Souers, R. T. Tsugawa, and E. M. Fearon, Chem. Phys. Lett. **81**, 26 (1981); J. D. Poll, J. L. Hunt, P. C. Souers, E. M. Fearon, R. T. Tsugawa, J. H. Richardson, and G. H. Smith, Phys. Rev. A **28**, 3147 (1983); M. A. Selen, R. L. Brooks, J. L. Hunt, J. D. Poll, Jack R. MacDonald, and J. C. Waddington, Nucl. Instrum. Methods **230**, 720 (1984).

[11]R. L. Brooks, J. L. Hunt, Jack R. MacDonald, J. D. Poll, and J. C. Waddington, Can. J. Phys. (to be published).

[12]J. D. Poll and J. L. Hunt, Can. J. Phys. **63**, 84 (1985).

[13]S. K. Bose and J. D. Poll, Can. J. Phys. **63**, 94 (1985).

[14]J. F. Ziegler, *Handbook of Stopping Cross-sections for Energetic Ions in All Elements* (Pergamon, Oxford, 1980).

[15]Scott L. Anderson, F. A. Houle, D. Gerlich, and Y. T. Lee, J. Chem. Phys. **75**, 2153 (1981).

[16]Inosuke Koyano and Kenichiro Tanaka, J. Chem. Phys. **72**, 4858 (1980).

[17]Charles H. Douglass, Donald J. McClure, and W. Ronald Gentry, J. Chem. Phys. **67**, 4931 (1977).

[18]J. Wm. McGowan, P. M. Mul, V. S. D'Angelo, J. B. A. Mitchell, P. Defrance, and H. R. Froelich, Phys. Rev. Lett. **42**, 373 (1979); **42**, 1186(E) (1979).

[19]Yukio Yamaguchi, Jeffrey F. Gaw, and Henry F. Schaefer III, J. Chem. Phys. **78**, 4074 (1983).

[20]A. Van Deursen and J. Reuss, Int. J. Mass. Spectrom. Ion Phys. **11**, 483 (1973).

[21]C. Ebner and C. C. Sung, Phys. Rev. A **5**, 2625 (1972).

[22]P. G. Le Comber, R. J. Loveland, and W. E. Spear, Phys. Rev. B **11**, 3124 (1975).

[23]P. G. LeComber, J. B. Wilson, and R. J. Loveland, Solid State Commun. **18**, 377 (1976).

[24]T. Holstein, Ann. Phys. (N.Y.) **8**, 343 (1959); D. Emin and T. Holstein, *ibid.* **53**, 439 (1969).